

Structure and Diffusion of Nanoparticle Monolayers Floating at Liquid/Vapor Interfaces: A Molecular Dynamics Study

Shengfeng Cheng* and Gary S. Grest
 Sandia National Laboratories, Albuquerque, NM 87185, USA
 (Dated: May 2, 2012)

Large-scale molecular dynamics simulations are used to simulate a layer of nanoparticles diffusing on the surface of a liquid. Both a low viscosity liquid, represented by Lennard-Jones monomers, and a high viscosity liquid, represented by linear homopolymers, are studied. The organization and diffusion of the nanoparticles are analyzed as the nanoparticle density and the contact angle between the nanoparticles and liquid are varied. When the interaction between the nanoparticles and liquid is reduced the contact angle increases and the nanoparticles ride higher on the liquid surface, which enables them to diffuse faster. In this case the short range order is also reduced as seen in the pair correlation function. For the polymeric liquids, the out-of-layer fluctuation is suppressed and the short range order is slightly enhanced. However, the diffusion becomes much slower and the mean square displacement even shows sub-linear time dependence at large times. The relation between diffusion coefficient and viscosity is found to deviate from that in bulk diffusion. Results are compared to simulations of the identical nanoparticles in 2-dimensions.

I. INTRODUCTION

Nanoparticles at a liquid/vapor or liquid/liquid interface have attracted extensive attention during the past two decades.¹ One motivation is that nanoparticles adsorbed at interfaces are found to be able to stabilize emulsions and foams.²⁻⁴ Nanoparticles also self-assemble into various structures at an interface, which provides an efficient route to produce superlattices of nanoparticles of technological importance.⁵⁻⁷ The advantage of this technique is that the assembly process can be fast and the resulting arrays are usually highly ordered. Due to their small size the adsorption energy of nanoparticles at an interface is typically only a few $k_B T$, where k_B is the Boltzmann constant and T is the temperature.^{1,5,8} The small adsorption energy implies that the adsorbed nanoparticles are highly dynamic and the self-assembly is quite reversible, the latter of which has been found to be crucial to form highly ordered arrays.^{6,9} Nanoparticles straddling an interface can also be regarded as living in a quasi 2-dimensional (2D) environment, which provides a model system to study interesting problems such as phase transitions of 2D fluids.¹⁰⁻¹³

Many experimental studies have been devoted to investigate the factors controlling the behavior of nanoparticles at an interface, including their size, surface morphology, shape, materials polarizability, and coatings.¹⁴⁻¹⁸ Some of these factors influence the location and orientation of individual nanoparticles; others influence their mutual interactions and assembly geometry. However, in experiments these factors are usually intertwined to yield collective effects and it is difficult to single out the effect of each factor alone. This aspect is where molecular dynamics (MD) simulations can play a useful role by studying the effect of one factor at a time to help elucidate experimental observations and uncover new physical insights.¹⁹⁻²⁷ For example, Bresme *et al.* showed that Young's equation can be used to describe force balance at nanoscale interfaces, but in certain cases line ten-

sion should also be included.¹⁹ Fenwick and Powell *et al.* showed that contrary to expectations, the collapse pressure measured in a typical Langmuir trough experiment should be independent of the contact angle.^{20,21} Recently, Cheung showed the importance of nanoparticle-liquid interactions and capillary waves in determining the stability of nanoparticles at liquid interfaces.²⁵

Although MD simulations to date have revealed many important aspects of the physical behavior of nanoparticles at an interface, some aspects are still unclear. Particularly, it is not clear how the structure and dynamics depend on contact angle and nanoparticle density in the low coverage regime. These behaviors are important since low density clusters can occur at the earlier stage of assembly and affect the morphology of the final dense layer.²⁸ The effect of liquid viscosity on interfacial diffusion is also not well understood and has only been studied recently.^{24,29} In this paper we use MD to study the structure and dynamics of a layer of nanoparticles floating at a liquid/vapor interface. We focus on the effect of varying the contact angle, which is controlled by interactions between the nanoparticles and liquid, the nanoparticle density, and the liquid viscosity, respectively. Snapshots of some of the systems we have simulated are shown in Fig. 1 (only a part of the full simulation box is shown in each case). In Fig. 1(a) the contact angle between the nanoparticle and liquid is $\theta_c = 137^\circ$. In this case the nanoparticles only slightly dip into the liquid which is composed of Lennard-Jones (LJ) monomers and is in equilibrium with its vapor phase. In Fig. 1(b) $\theta_c = 29^\circ$ and the nanoparticles are almost immersed in the liquid. In Fig. 1(c) $\theta_c = 93^\circ$ and the nanoparticles straddle the surface of the liquid, in this case composed of flexible linear polymer chains. Note that the LJ monomer liquid has a high vapor density, but the vapor density of the polymeric liquid is essentially 0.³⁰ Also note that the polymeric liquid has a higher bulk density than that of the monatomic liquid and the liquid film in Fig. 1(c) is thinner than those in Fig. 1(a) and (b) since in our simu-

lations all liquids contain a similar number of monomers.

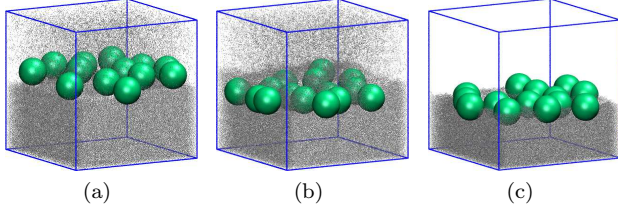


FIG. 1: (Color online) Snapshots of nanoparticles floating at liquid/vapor interfaces: (a) monatomic LJ liquid and $\theta_c = 137^\circ$; (b) monatomic LJ liquid and $\theta_c = 29^\circ$; (c) 100-bead chain polymeric liquid and $\theta_c = 93^\circ$. Only a small portion ($100\sigma \times 100\sigma \times 100\sigma$) of the simulation cell is shown in each snapshot.

II. SIMULATION METHODOLOGY

We placed a layer of nanoparticles at a liquid/vapor interface as shown in Fig. 1. Three liquid systems consisting of either LJ monomers or flexible linear chains of N LJ beads for $N = 10$ and 100 were studied. In all three cases, the beads interact with each other through the standard LJ 12-6 potential

$$U_{\text{LJ}}(r) = 4\epsilon \left[\left(\frac{\sigma}{r} \right)^{12} - \left(\frac{\sigma}{r} \right)^6 - \left(\frac{\sigma}{r_c} \right)^{12} + \left(\frac{\sigma}{r_c} \right)^6 \right], \quad (1)$$

where r is the distance between two beads, ϵ is the unit of energy, and σ is the diameter of beads. The interaction is truncated at $r_c = 3.0\sigma$. For the two polymeric liquids, beads in the chain are connected by an additional finite extensible nonlinear elastic potential with a spring constant $k = 30\epsilon/\sigma^2$ and maximum extent $R_0 = 1.5\sigma$.³¹ The liquid density ρ and shear viscosity η for the LJ monomer liquid is $\rho = 0.66\sigma^{-3}$ and $\eta = 1.01 \pm 0.03m/\tau\sigma$,³² while for the polymer liquids, $\rho = 0.89\sigma^{-3}$ and $\eta = 12 \pm 1m/\tau\sigma$ for $N = 10$, and $\rho = 0.91\sigma^{-3}$ and $\eta = 180 \pm 10m/\tau\sigma$ for $N = 100$.^{33,34}

The nanoparticles are assumed to consist of a uniform distribution of atoms interacting with a LJ potential. For spherical particles, their mutual interaction can then be determined analytically by integrating over all the interacting LJ atom pairs between the two particles.^{35,36} For nanoparticles with radii a , the interaction energy is given by

$$U_{\text{nn}}(r) = -\frac{A_{\text{nn}}}{6} \left[\frac{2a^2}{r^2 - 4a^2} + \frac{2a^2}{r^2} + \ln \left(\frac{r^2 - 4a^2}{r^2} \right) \right] + \frac{A_{\text{nn}}}{37800} \frac{\sigma_n^6}{r} \left[\frac{r^2 - 14ra + 54a^2}{(r - 2a)^7} + \frac{r^2 + 14ra + 54a^2}{(r + 2a)^7} - \frac{2(r^2 - 30a^2)}{r^7} \right]. \quad (2)$$

Here r is the center-to-center distance between two nanoparticles. The Hamaker constant $A_{\text{nn}} = 4\pi^2\epsilon_{\text{nn}}\rho_n^2\sigma_n^6$, where ϵ_{nn} is the interaction strength between the LJ atoms that make up the nanoparticles, and

σ_n is the diameter and ρ_n the density of LJ atoms in the nanoparticles. To reduce the number of parameters, we take $\epsilon_{\text{nn}} = \epsilon$, $\sigma_n = \sigma$ and $\rho_n = 1.0\sigma^{-3}$, in which case $A_{\text{nn}} = 39.48\epsilon$. In this paper we set $a = 10\sigma$.

The interaction between the LJ beads and nanoparticles is determined by integrating the interaction between a LJ bead and the LJ atoms within a nanoparticle, and the interaction potential $U_{\text{ns}}(r)$ is given by

$$U_{\text{ns}}(r) = \frac{2}{9} \frac{a^3\sigma_n^3 A_{\text{ns}}}{(a^2 - r^2)^3} \times \left[1 - \frac{(5a^6 + 45a^4r^2 + 63a^2r^4 + 15r^6)\sigma_n^6}{15(a^2 - r^2)^6} \right], \quad (3)$$

where r is the center-to-center distance between the bead and nanoparticle, and the Hamaker constant $A_{\text{ns}} = 24\pi\epsilon_{\text{ns}}\rho_n\sigma_n^3 = 24\pi\epsilon_{\text{ns}}$ for $\sigma_n = \sigma$ and $\rho_n = 1.0\sigma^{-3}$.

Depending on the values of the Hamaker constant A_{nn} and A_{ns} , the nanoparticles can either be dispersed in the liquid or phase separate. As we are interested in studying nanoparticles that are hard-sphere like at the liquid/vapor surface, we truncate the nanoparticle-nanoparticle interaction so that it is purely repulsive. For $a = 10\sigma$, this gives a cutoff $r_c = 20.427\sigma$ for $U_{\text{nn}}(r)$. Physically this corresponds to adding a short surfactant coating to the nanoparticles to avoid flocculation.^{37,38} For the interaction between the nanoparticles and LJ beads making up the liquid and vapor, we set $r_c = a + 4\sigma = 14\sigma$. The remaining free parameter A_{ns} controls the solubility of the nanoparticles in the liquid. We choose A_{ns} such that nanoparticles phase separate to the liquid/vapor interface, in which case A_{ns} controls the contact angle θ_c of the nanoparticles on the liquid surface. Results for θ_c as a function of A_{ns} are shown in Fig. 2. The data show that $\theta_c \rightarrow 180^\circ$ as $A_{\text{ns}} \rightarrow 0$. However, when A_{ns} exceeds certain critical value, which is approximately 85ϵ for LJ monomers and 120ϵ (130ϵ) for 10-bead (100-bead) chains, θ_c goes to 0 and the nanoparticles diffuse into the liquid. In the intermediate range around 90° , θ_c decreases roughly linearly as A_{ns} increases. For a fixed A_{ns} , θ_c increases as the chain length increases. This trend can be qualitatively understood as the result of less entropy gain when mixing the nanoparticles with longer chains. Correspondingly, a larger A_{ns} , which represents the enthalpy contribution of solvation, is required to disperse the nanoparticles into a liquid of longer chains.³⁹ The effects of A_{ns} and chain length on the behavior of the nanoparticles at the liquid/vapor interface are visualized in Fig. 1.

All MD simulations were performed using the LAMMPS simulation package.^{40,41} The simulation cell is a rectangular box of dimensions $L_x \times L_y \times L_z$, where $L_x = 390.577\sigma$, $L_y = 451.0\sigma$, and $L_z = 120\sigma$ for the LJ monomer liquid and 70σ for the polymeric liquids. The liquid/vapor interface is parallel to the x - y plane, in which periodic boundary conditions were employed. In the z direction, the LJ atoms and nanoparticles are confined by two flat walls at $z = 0$ and $z = L_z$, respectively. Since the 2D packing of hard spheres is very sensitive to the aspect ratio of the enclosing box, we set

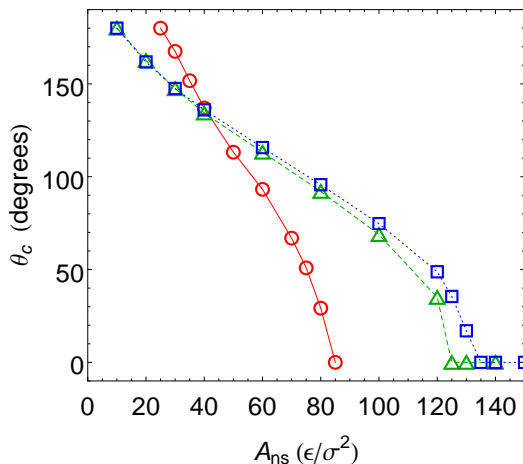


FIG. 2: (Color online) Contact angle θ_c vs. nanoparticle-liquid interaction strength A_{ns} for different liquids: monatomic LJ liquid (circles), 10-bead chain polymeric liquid (triangles), and 100-bead chain polymeric liquid (squares). Uncertainties in θ_c are $\sim 1^\circ - 2^\circ$, smaller than the symbol size. Lines are guides to the eye.

$L_x/L_y = \sqrt{3}/2$ so that the hexagonal close-packing is favored. Each system contains more than 6 million LJ atoms to form a liquid layer with a thickness $\sim 50\sigma$ and in equilibrium with its vapor phase, which in the LJ monomer case has a thickness $\sim 70\sigma$ for $L_z = 120\sigma$. For the polymeric liquids, the vapor density is 0 and L_z was reduced accordingly. In order to investigate the effect of nanoparticle coverage, three systems were simulated with $N_p = 200, 240$, and 320 nanoparticles, corresponding to 2D density $\phi \equiv N_p(2a)^2/(L_x L_y) = 0.45, 0.54$, and 0.73 , respectively. All these densities are well below the critical density 0.89 at the liquid/hexatic transition and 0.92 at the hexatic/solid transition of 2D hard disk fluids.^{42–44}

The LJ atoms interact with both upper and lower walls through a LJ 9-3 potential, which depends only on their distance z from the wall,

$$U(z) = \epsilon_w \left[\frac{2}{15} \left(\frac{\sigma}{z} \right)^9 - \left(\frac{\sigma}{z} \right)^3 - \frac{2}{15} \left(\frac{\sigma}{z_c} \right)^9 + \left(\frac{\sigma}{z_c} \right)^3 \right], \quad (4)$$

where $\epsilon_w = 2\epsilon$. For the lower wall the interaction is truncated at $z_c = 3.0\sigma$, while at the upper wall is purely repulsive with $z_c = 0.71476\sigma$. Though all nanoparticles are confined to the liquid/vapor interface and far from the two walls in most simulations, we also included a nanoparticle-wall potential of the form

$$U(z) = A_{nw} \left[\frac{\sigma^6}{7560} \left(\frac{7a-z}{(z-a)^\tau} + \frac{7a+z}{(z+a)^\tau} \right) - \frac{1}{6} \left(\frac{2az}{z^2-a^2} + \ln \frac{z-a}{z+a} \right) \right], \quad (5)$$

where z is the distance of the center of a nanoparticle from the wall and $A_{nw} = 144\epsilon$. At both walls the potential is truncated at $z = 10.57187\sigma$ to make it purely repulsive for the nanoparticles. This potential is useful

for larger values of A_{ns} where the nanoparticles are dispersed in the liquid.³⁸

The equations of motion were integrated using a velocity-Verlet algorithm with a time step $\delta t = 0.005\tau$, where $\tau = \sigma(m/\epsilon)^{1/2}$ and m is the mass of a LJ monomer. The nanoparticle with a radius $a = 10\sigma$ has a mass $M = \frac{4\pi a^3 m}{3\sigma^3} = 4188.79m$. During the equilibration, the temperature T was held at $1.0\epsilon/k_B$ by a Langevin thermostat weakly coupled to all LJ atoms with a damping constant $\Gamma = 0.1\tau^{-1}$. Once the liquid/vapor interface was equilibrated, the Langevin thermostat was removed except for those liquid atoms within 10σ of the lower wall at $z = 0$. Since the thickness of the liquid layer is $\sim 50\sigma$ and all nanoparticles are floating at the liquid/vapor interface in our simulations, their motion is not affected by the thermostat.

For comparison, we also conducted MD simulations of 5000 nanoparticles in a 2D box with $L_x/L_y = 1$. The size of the 2D box was varied to ensure the same density as for the nanoparticles at liquid/vapor interfaces. A Langevin thermostat with a damping constant $\Gamma = 0.1\tau^{-1}$ was used to keep the temperature at $T = 1.0\epsilon/k_B$. The thermostat works as an implicit solvent. The interaction between the nanoparticles is still given by Eq. (2) since capillary interactions are negligible for nanoparticles because of the irrelevance of gravity.⁴⁵ We confirmed this treatment in our simulations by directly calculating and visualizing the liquid/vapor interface, which is flat (except for temporary capillary fluctuations) all the way to the contact line on the nanoparticle surface and shows no distortion at all with the presence of nanoparticles. It should be pointed out that for larger particles, capillary interactions can be taken into account even in 2D simulations by adding an effective capillary attraction between particles.⁴⁶

III. RESULTS AND DISCUSSION

A. Out-of-Plane Fluctuations

At a finite contact angle θ_c , the nanoparticles straddle the liquid/vapor interface and form a layer that is essentially 2D, with small thermal fluctuations in the z -direction normal to the interface. Direct calculation of the magnitude of fluctuations shows that it is almost independent of θ_c and the nanoparticle density ϕ , but strongly depends on the properties of the supporting liquid film, including its density, viscosity, and surface tension. Because of thermal fluctuations, the layer thickness is broadened and the individual nanoparticle height deviates from the mean value of all nanoparticles. Such deviations are apparent in snapshots shown in Fig. 1. More quantitative results are shown in Fig. 3, where the probability density distribution $P(\delta z_p)$ is calculated as a function of the deviation δz_p from the instantaneous mean height of all nanoparticles. Note that the mean height itself fluctuates with time, but such fluctuations are excluded in Fig. 3. Including them would make the

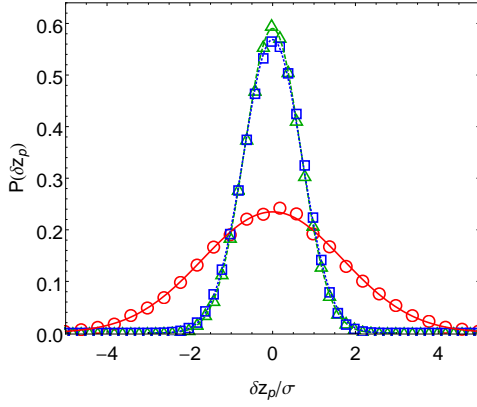


FIG. 3: (Color online) Probability density distribution $P(\delta z_p)$ of nanoparticle positions in the z -direction, where δz_p is the deviation of position from the instantaneous mean of all nanoparticles. Data are for $\phi = 0.54$, $\theta_c = 93^\circ$, and various liquids: monatomic LJ liquid (circles), 10-bead chain polymeric liquid (triangles), and 100-bead chain polymeric liquid (squares). Lines are the corresponding Gaussian fits.

distributions even wider. The distributions in Fig. 3 all have a Gaussian shape, with a variance $(1.75 \pm 0.08)\sigma$ for the monatomic LJ liquid, and $\sim 0.7\sigma$ for the two polymeric liquids. Since the nanoparticle diameter is 20σ , the height variations amongst the nanoparticles are less than 10% of their diameter, which confirms that the nanoparticle layer is close to a 2D system.

B. In-Plane Structure

To characterize the structure in the plane of the nanoparticle layer, we computed the 2D radial distribution function $g(r)$ and the structure factor $S(\mathbf{q})$, where $\mathbf{q} = q_x e_x + q_y e_y$ is a 2D wave-vector and e_x and e_y are unit vectors along x and y directions, respectively. While $g(r)$ and $S(\mathbf{q})$ are related through a Fourier transform, for a finite system it is easier to calculate each one directly. The calculation of $g(r)$ involves counting the number of pairs of nanoparticles separated by distance r and is straightforward. The structure factor is given by

$$S(\mathbf{q}) = N_p^{-1} \sum_{m,n} \exp(i\mathbf{q} \cdot \mathbf{r}_{mn}), \quad (6)$$

where the sum is taken over all nanoparticle pairs indexed by m and n and separated by $\mathbf{r}_{mn} = \mathbf{r}_m - \mathbf{r}_n$.

Results of $g(r)$ are shown in Fig. 4. Data in Fig. 4(a) are for different ϕ 's at $\theta_c = 93^\circ$. These results show the expected increase in the height of the first peak in $g(r)$ as ϕ increases. The effect of θ_c on $g(r)$ is illustrated in Fig. 4(b)-(d). All results consistently show that when θ_c is reduced, the locations of the peaks of $g(r)$ move to larger r , which indicates that the nanoparticle layer is slightly denser at larger θ_c . This trend is consistent with experimental results on the silica nanoparticle layer at the water-air interface.¹⁷ It can be understood from

a simple physical picture. At large θ_c , the nanoparticles ride high at the liquid/vapor interface and the separation between nanoparticles is solely controlled by the hard core repulsion. However, at small θ_c , the nanoparticles are partially coated by the liquid, which increases their effective size. So as θ_c decreases the mean separation between two nanoparticles increases.

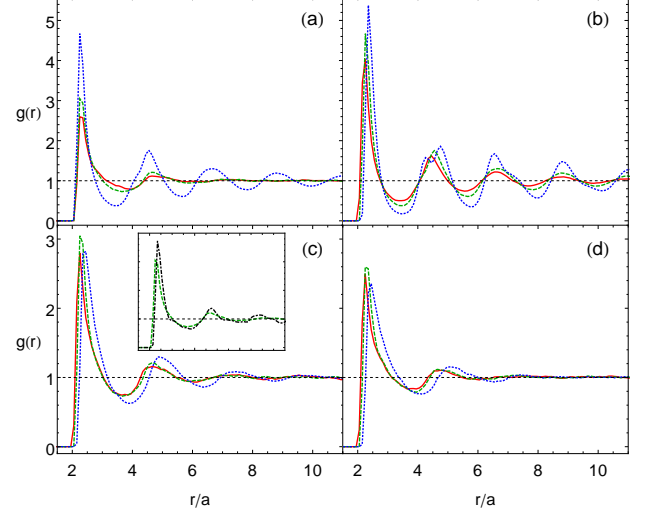


FIG. 4: (color online) The pair distribution function $g(r)$. Lines in all main panels are for the monatomic LJ liquid: (a) $\theta_c = 93^\circ$ and $\phi = 0.45$ (solid), 0.54 (dashed), 0.73 (dotted); (b) $\phi = 0.73$ and $\theta_c = 137^\circ$ (solid), 93° (dashed), 51° (dotted); (c) $\phi = 0.54$ and $\theta_c = 137^\circ$ (solid), 93° (dashed), 51° (dotted); (d) $\phi = 0.45$ and $\theta_c = 137^\circ$ (solid), 93° (dashed), 51° (dotted). Inset of (b): The dashed line is for the monatomic LJ liquid and the dash-dotted line is for the polymeric liquid consisting of 100-bead chains; for both lines $\phi = 0.54$ and $\theta_c = 93^\circ$;

Figure 4(b) shows that at $\phi = 0.73$ the peaks of $g(r)$ grow as θ_c decreases, indicating that the nanoparticle layer becomes more ordered at smaller θ_c . The data in Fig. 4(c) and (d) for $\theta_c = 137^\circ$ and 93° also show this trend. However, the first peak of $g(r)$ becomes lower when θ_c is further reduced to 51° , though other peaks become higher. The apparent reduction in the first peak of $g(r)$ at $\theta_c = 51^\circ$ is due to a finite size effect. The calculation of $S(\mathbf{q})$ indicates that all peaks grow as θ_c decreases and confirms that the nanoparticle layer exhibits stronger local order at smaller θ_c .

As θ_c continues to decrease to 0, we have observed the loss of nanoparticles at the interface as some of them diffuse into the liquid, though θ_c for an individual nanoparticle may still be finite. This effect is more significant at higher nanoparticle density. For example, at $\theta_c = 29^\circ$ more than 18% nanoparticles were dispersed in the liquid at the end of MD runs for $\phi = 0.73$; while for $\phi = 0.45$, about 8% have diffused into the liquid. The loss of nanoparticles at the interface for a finite θ_c is a consequence of their small activation energy, which is typically at the order of several $k_B T$.¹

Result of $g(r)$ for the polymeric liquid consisting of 100-bead chains is included in the inset of Fig. 4(c), together with the result for the monatomic LJ liquid at the same θ_c and ϕ . The peaks of $g(r)$ are slightly higher for the polymeric liquid than those for the monatomic LJ liquid, indicating that local order is slightly stronger in the former case. As shown in Fig. 3, the out-of-layer fluctuation is much smaller for the polymeric liquids, i.e., the nanoparticle layer is more 2D-like. As a consequence, the nanoparticle density is effectively higher, which leads to higher peaks in $g(r)$ for the polymeric liquids.

A comparison of $g(r)$ for nanoparticles at the liquid/vapor interface and in 2D with an implicit solvent is shown in Fig. 5 for three densities. The peaks in $g(r)$ for nanoparticles at the interface are clearly higher and decay slower than those for nanoparticles in 2D, indicating stronger local order in the former case. The locations of the peaks move towards larger r for nanoparticles at the interface. The shift is between 2 to 2.5σ , and reflects the liquid coating that is about 1σ in thickness on each nanoparticle. The coating makes the nanoparticles effectively larger than the bare ones in 2D simulations. Therefore, the actual nanoparticle density is effectively higher at the interface, which leads to higher peaks in $g(r)$. However, if the radius of nanoparticles in 2D was increased to reflect this coating, then we would expect higher peaks in $g(r)$ at a given ϕ from 2D simulations. This trend can be derived indirectly from the previous comparison of $g(r)$ between the monatomic LJ liquid and polymeric liquids. Higher peaks are found for the latter since the nanoparticle layer there is more 2D-like.

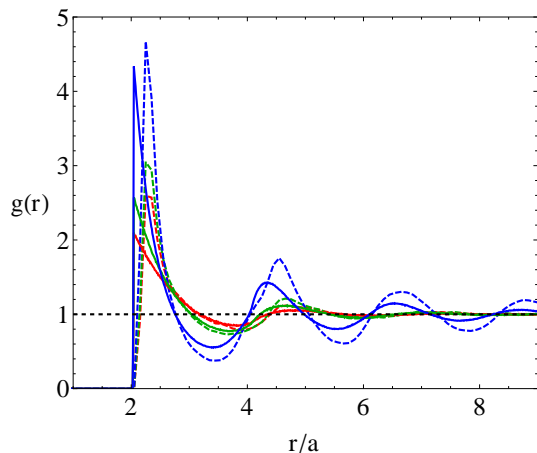


FIG. 5: (color online) The pair distribution function $g(r)$ for nanoparticles at the liquid/vapor interface for the LJ monatomic liquid at $\theta_c = 93^\circ$ (dashed lines) compared to results of 2D simulations (solid lines) for $\phi = 0.45$ (bottom), 0.54 (middle), and 0.73 (top).

Additional information on the in-plane structure of the nanoparticle layer can be obtained from $S(\mathbf{q})$. A density plot of $S(\mathbf{q})$ in the q_x - q_y plane is shown in Fig. 6 for $\theta_c = 93^\circ$ and the monatomic LJ liquid at $\phi = 0.54$ and 0.73 , and the 100-bead chain polymeric liquid at

$\phi = 0.54$. At low density $\phi = 0.45$ and 0.54 , the local structure is almost isotropic, indicating a fluid-like state of the floating layer. However, at $\phi = 0.73$, which is still lower than the critical density for the fluid/solid transition of 2D hard sphere systems, the hexagonal close-packing feature of the local structure is rather apparent as shown in the middle panel of Fig. 6. Smaller out-of-plane fluctuations of nanoparticles on the surface of the polymeric liquid lead to stronger local order in the nanoparticle layer at a given ϕ and θ_c , indicated by higher peaks in $S(\mathbf{q})$.

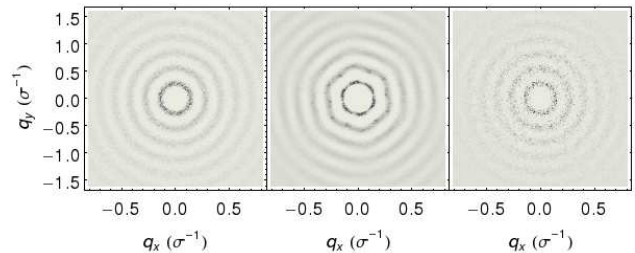


FIG. 6: (color online) Density plots of $S(\mathbf{q})$ in the q_x - q_y plane for $\theta_c = 93^\circ$ and the monatomic LJ liquid at $\phi = 0.54$ (left) and 0.73 (middle), and the 100-bead chain polymeric liquid at $\phi = 0.54$ (right).

C. Orientational Order

A simple measure of orientational order of the floating nanoparticle layer is provided by the fraction of nanoparticles, f_6 , which have exactly six neighbors as in a close-packed hexagonal lattice. Here a simple criterion is adopted to identify nearest neighbors as those within a cut-off radius r_c of a given nanoparticle. We chose $r_c = 35\sigma$, roughly corresponding to the location of the first valley of $g(r)$ as shown in Fig. 4. After nearest neighbors were found, we computed the Nelson-Halperin (N-H) order parameter, which can be expressed as

$$m_6 = \left\langle \left| \frac{1}{N_p} \sum_{j=1}^{N_p} \frac{1}{n_j} \sum_{k=1}^{n_j} \exp(i6\theta_{jk}) \right| \right\rangle, \quad (7)$$

where the first sum is over all N_p nanoparticles, n_j is the number of nearest neighbors of the j -th nanoparticle, the second sum is over n_j nearest neighbors, and θ_{jk} is the angle formed by the bond between a nearest neighbor pair (j, k) and a fixed axis. For an ideal hexagonal lattice $m_6 = 1$, and it decreases to zero as the local bond disorder increases.

Results of f_6 and m_6 vs. ϕ are shown in Fig. 7 for nanoparticles floating on the surface of the monatomic LJ liquid at various contact angles. Results of 2D simulations are also included. As expected, in all cases f_6 and m_6 increase with ϕ , indicating the development of orientational order. Figure 7 also shows that at a given ϕ , the layer is more locally ordered at smaller θ_c as indicated by larger values of m_6 and f_6 . The increase in

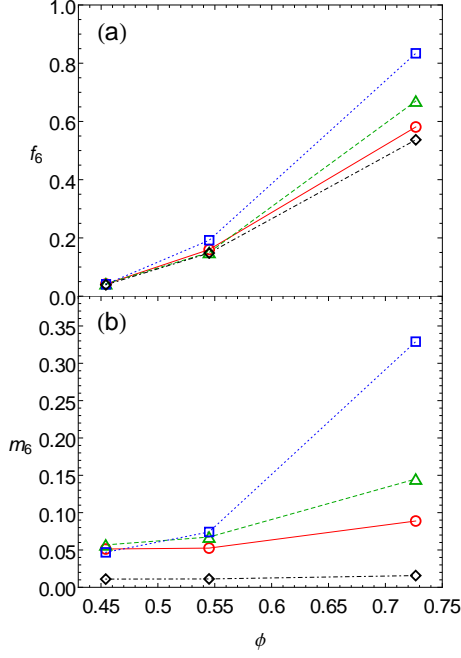


FIG. 7: (a) The fraction of nanoparticles, f_6 , having exactly six neighbors and (b) the N-H order parameter m_6 vs. the nanoparticle density ϕ for nanoparticles on the surface of the monatomic LJ liquid at various contact angles: $\theta_c = 137^\circ$ (circles); $\theta_c = 93^\circ$ (triangles); $\theta_c = 51^\circ$ (squares). Results of 2D simulations are shown with diamonds. Lines are guides to the eye.

orientational order as θ_c is reduced is more dramatic at higher ϕ . This trend persists in our simulations when θ_c is reduced even further (e.g., $\theta_c = 29^\circ$). In this case since some nanoparticles are eventually absorbed into the liquid at long times, we can only calculate f_6 and m_6 in the early stages of simulations when all nanoparticles are still at the liquid/vapor interface. In this early time regime systems follow the same trend that at a given ϕ , values of f_6 and m_6 are larger and the order is stronger at smaller θ_c . The trend is consistent with that found from $g(r)$ as shown in Fig. 4. Data in Fig. 7 also show that orientational order is stronger for nanoparticles at the interface than for those in 2D since the liquid coating in the former case makes nanoparticles effectively larger and their density higher. The same reason also leads to enhancement of translational order as shown in Fig. 5.

The N-H order parameter m_6 shown in Fig. 7 was calculated with nearest neighbors identified with a simple cut-off criterion. To verify that this criterion leads to an accurate estimate of orientational order, we also conducted a Voronoi analysis of the packing geometry of the nanoparticle layer.⁴⁷ Nearest neighbors were identified as those sharing common sides in the Voronoi construction. The N-H order parameter was then computed with Eq. (7). Results from the Voronoi analysis typically agree within a few percent with those from the simpler cut-off approach. Thus the cut-off criterion is adequate

for finding nearest neighbors needed for the calculation of the N-H order parameter, even when the nanoparticle density is low.

D. Diffusion Coefficient

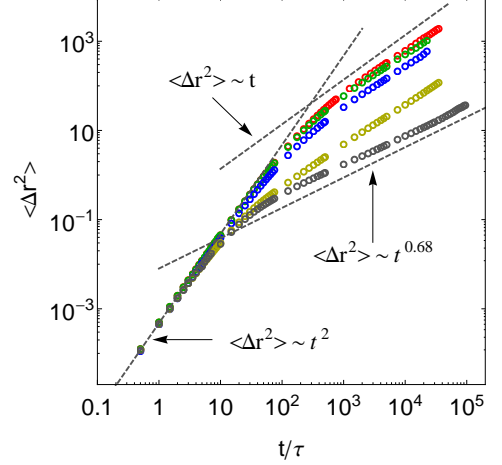


FIG. 8: (a) Mean square displacement $\langle \Delta r^2 \rangle$ vs. time t . The top three data sets are for the monatomic LJ liquid at $\phi = 0.45$ and $\theta_c = 137^\circ$; $\phi = 0.54$ and $\theta_c = 137^\circ$; $\phi = 0.54$ and $\theta_c = 93^\circ$. The second to bottom (bottommost) data set is for the polymeric liquid consisting of 10-bead (100-bead) chains at $\phi = 0.54$ and $\theta_c = 93^\circ$.

The in-plane motion of nanoparticles at the liquid/vapor interface is characterized by the mean square displacement $\langle \Delta r^2 \rangle \equiv \langle \Delta x^2 + \Delta y^2 \rangle$, which is shown in Fig. 8 for various cases. At very short times, the motion of nanoparticles is nearly ballistic with $\langle \Delta r^2 \rangle = v^2 t^2$, where v is a velocity and t is time. At larger times, the motion becomes diffusive and $\langle \Delta r^2 \rangle = 4Dt$, where D is a diffusion coefficient and 4 is the prefactor for 2D diffusion. Most of our results fit to this classical picture, as shown in Fig. 8. In all cases, $v \simeq 0.02\sigma/\tau$ and is nearly independent of θ_c and ϕ . The intersection of the ballistic and diffusive regime defines a ballistic time scale $t_b = 4D/v^2$. Results for D and t_b are shown in Fig. 9 as a function of the true nanoparticle density $\tilde{\phi}$ for 4 values of θ_c . At small θ_c (e.g., $\theta_c = 29^\circ$), because of the loss of nanoparticle from the interface, $\tilde{\phi}$ is lower than the nominal density ϕ calculated from N_p . In other cases $\tilde{\phi} = \phi$. Figure 9 shows that in all cases, D and t_b decrease approximately linearly with the nanoparticle density and the slope is steeper for larger θ_c . At the same $\tilde{\phi}$, both D and t_b decrease as θ_c decreases. This is due to the fact that the attraction between the nanoparticles and liquid is enhanced to make θ_c smaller. As a consequence, nanoparticles become more immersed into the liquid and need to plow through more liquid in order to move, which makes their diffusion more difficult. At $\tilde{\phi} = 0.45$, D and t_b decrease by a factor of 3 when θ_c is reduced from 137°

to 29° . At $\tilde{\phi} = 0.73$, the reduction is almost 6-fold for the same change in θ_c .

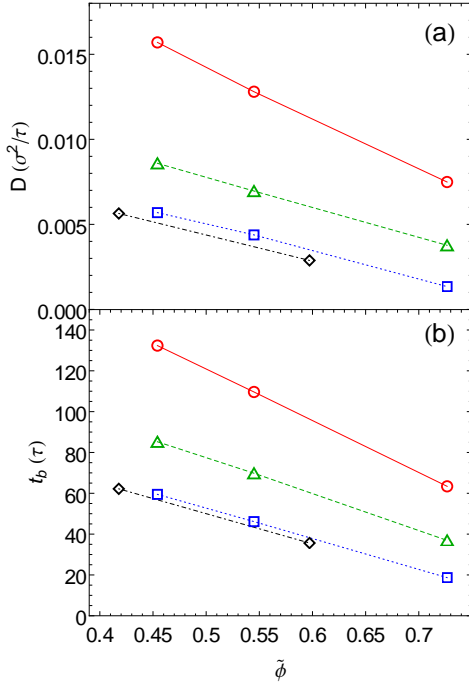


FIG. 9: (a) Diffusion coefficient D and (b) ballistic time t_b vs. the true nanoparticle density $\tilde{\phi}$ at various contact angles: $\theta_c = 137^\circ$ (circles), $\theta_c = 93^\circ$ (triangles), $\theta_c = 51^\circ$ (squares), $\theta_c = 29^\circ$ (diamonds). $\tilde{\phi}$ is the same as ϕ except for $\theta_c = 29^\circ$, where $\tilde{\phi} < \phi$. Lines are guides to the eye.

For the 10-bead chain polymeric liquid, $\langle \Delta r^2 \rangle$ grows linearly with t^2 at early times and shows diffusive behavior at large times. However the diffusion coefficient is reduced significantly compared to the LJ monomer case. For example, at $\tilde{\phi} = 0.54$ and $\theta_c = 93^\circ$, the value of D is $\sim 1 \times 10^{-3} \sigma^2/\tau$ for the 10-bead polymeric liquid compared to $\sim 7 \times 10^{-3} \sigma^2/\tau$ for the monatomic LJ liquid. Note that Fig.2 shows that the interaction strength between the nanoparticles and liquid, dictated by A_{ns} , has to be adjusted to ensure the same θ_c for the polymeric and monatomic LJ liquid. For example, $\theta_c = 93^\circ$ for the monatomic LJ liquid at $A_{ns} = 60\epsilon/\sigma^2$, while we need to increase A_{ns} to $79\epsilon/\sigma^2$ to get the same θ_c for the 10-bead polymeric liquid. If A_{ns} is held fixed at $A_{ns} = 60\epsilon/\sigma^2$ for the 10-bead polymeric liquid, then θ_c increases to 113° . In this case D is $\sim 1.6 \times 10^{-3} \sigma^2/\tau$. These data are summarized in Table I. If we compare the values of D between the monatomic LJ and 10-bead polymeric liquid at $A_{ns} = 60\epsilon/\sigma^2$, i.e., at the same nanoparticle-bead interaction, we find that D is reduced by a factor about 4. Note that the viscosity η of the 10-bead polymeric liquid is approximately 12 times larger than that of the monatomic LJ liquid. If we assume a scaling relation between D and η as $D \sim \eta^{-\alpha}$, then $\alpha \simeq 0.6$ is much less than 1, which is in contrast with the situation of free bulk Brownian diffusion where $\alpha = 1$ is expected.

liquid	$A_{ns} (\epsilon/\sigma^2)$	$\theta_c (^\circ)$	$\eta (m/\sigma\tau)$	$D (\sigma^2/\tau)$
monatomic	60	93	1.01	7.0×10^{-3}
10-bead	60	113	12	1.6×10^{-3}
10-bead	79	93	12	1.0×10^{-3}

TABLE I: Comparison of values of contact angle (θ_c), viscosity (η), and diffusion coefficient (D) at $\phi = 0.54$ for the monatomic LJ and 10-bead polymeric liquid.

However, our results are consistent with a recent experimental measurement of the diffusion coefficient of single nanoparticles at water-oil interfaces, where $\alpha = 0.44$ was found.²⁹

For the 100-bead chains, $\langle \Delta r^2 \rangle \sim t^2$ at early times, and then crosses over to a sub-diffusive regime as shown in Fig. 8. This deviation from the expected long-time linear dependence on time continued out to the longest times we are presently able to simulate. In this sub-diffusive regime, the mean square displacement for the 100-bead chains can be better fit to $\langle \Delta r^2 \rangle \sim t^{0.68}$, as shown in Fig. 8. The reason underlying this sub-diffusive regime is unclear.

V. CONCLUSIONS

In this paper we studied nanoparticles floating at liquid/vapor interfaces with MD simulations. Both the low-viscous monatomic LJ liquid and the high-viscous polymeric liquids composed of flexible linear chains were studied. We showed that as the attraction between the nanoparticles and liquid is increased, the contact angle is reduced and the nanoparticles are more wetted by the liquid. At the same time the short range order of the nanoparticle layer is slightly enhanced and the interfacial diffusion coefficient of the nanoparticles is greatly reduced. Our results further showed that both the translational and orientational order of the nanoparticle layer grow quickly and the nanoparticle diffusion slows down dramatically as the nanoparticle density is increased. Comparisons with results of 2D simulations revealed that the main effect of liquid on the nanoparticles is to provide a coating which makes their effective size larger than that of the bare ones. Otherwise, the nanoparticle layer at the liquid/vapor interface is close to a 2D system, though the out-of-plane fluctuations can be as large as 10% of their diameter. The simulations with more viscous polymeric liquids showed that the out-of-plane fluctuations of the nanoparticles are strongly suppressed even for relatively short chains (e.g., 10-bead chains). The local, short range order is slightly enhanced at a given contact angle and nanoparticle density as the chain length increases. At the same time, the nanoparticle diffusion becomes slower for more viscous liquids and even shows sub-diffusive behavior at large times for highly viscous liquids. The diffusion coefficient scales inversely with the viscosity however with an exponent less than 1.

ACKNOWLEDGMENTS

This research used resources of the National Energy Research Scientific Computing Center (NERSC), which is supported by the Office of Science of the United States Department of Energy under Contract No. DE-AC02-05CH11231, and the Oak Ridge Leadership Computing Facility located in the National Center for Computational Sciences at Oak Ridge National Laboratory, which is supported by the Office of Science of the United States Department of Energy under Contract No. DE-AC05-00OR22725. These resources were obtained through

the Advanced Scientific Computing Research (ASCR) Leadership Computing Challenge (ALCC). This work was supported by the Laboratory Directed Research and Development program at Sandia National Laboratories. Sandia National Laboratories is a multi-program laboratory managed and operated by Sandia Corporation, a wholly owned subsidiary of Lockheed Martin Corporation, for the U.S. Department of Energy's National Nuclear Security Administration under contract DE-AC04-94AL85000.

-
- * Electronic address: sncheng@sandia.gov
- ¹ F. Bresme and M. Oettel, *J. Phys.: Condens. Matter* **19**, 413101 (2007).
 - ² B. P. Binks and S. O. Lumsdon, *Langmuir* **16**, 8622 (2000).
 - ³ B. P. Binks and J. H. Clint, *Langmuir* **18**, 1270 (2002).
 - ⁴ T. S. Horozov and B. P. Binks, *Angew. Chem. Int. Ed.* **45**, 773 (2006).
 - ⁵ Y. Lin, H. Skaff, T. Emrick, A. D. Dinsmore, and T. P. Russell, *Science* **299**, 226 (2003).
 - ⁶ W. H. Binder, *Angew. Chem. Int. Ed.* **44**, 5172 (2005).
 - ⁷ A. Böker, J. He, T. Emrick, and T. P. Russell, *Soft Matter* **3**, 1231 (2007).
 - ⁸ K. Du, E. Glogowski, T. Emrick, T. P. Russell, and A. D. Dinsmore, *Langmuir* **26**, 12518 (2010).
 - ⁹ G. M. Whitesides and B. Grzybowski, *Science* **295**, 2418 (2002).
 - ¹⁰ P. Pieranski, *Phys. Rev. Lett.* **45**, 569 (1980).
 - ¹¹ T. Terao and T. Nakayama, *Phys. Rev. E* **60**, 7157 (1999).
 - ¹² K. Zahn and G. Maret, *Phys. Rev. Lett.* **85**, 3656 (2000).
 - ¹³ J. Sun and T. Stirner, *Phys. Rev. E* **67**, 051107 (2003).
 - ¹⁴ J. R. Heath, C. M. Knobler, and D. V. Leff, *J. Phys. Chem. B* **101**, 189 (1997).
 - ¹⁵ N. Glaser, D. J. Adams, A. Böker, and G. Krausch, *Langmuir* **22**, 5227 (2006).
 - ¹⁶ L. Isa, F. Lucas, R. Wepf, and E. Reimhult, *Nature Comm.* **2**, 438 (2011).
 - ¹⁷ D. Y. Zang, E. Rio, G. Delon, D. Langevin, B. Wei, and B. P. Binks, *Mol. Phys.* **109**, 1057 (2011).
 - ¹⁸ K. D. Comeau and M. V. Meli, *J. Chem. Phys.* **28**, 377 (2012).
 - ¹⁹ F. Bresme and N. Quirke, *Phys. Rev. Lett.* **80**, 3791 (1998).
 - ²⁰ N. I. D. Fenwick, F. Bresme, and N. Quirke, *J. Chem. Phys.* **114**, 7274 (2001).
 - ²¹ C. Powell, N. Fenwick, F. Bresme, and N. Quirke, *Colloids Surfaces A* **206**, 241 (2002).
 - ²² F. Bresme, H. Lehle, and M. Oettel, *J. Chem. Phys.* **130**, 214711 (2009).
 - ²³ C. Chiu, B. M. P. W. Shinoda, and S. O. Nielsen, *J. Chem. Phys.* **131**, 244706 (2009).
 - ²⁴ D. L. Cheung, *Chem. Phys. Lett.* **495**, 55 (2010).
 - ²⁵ D. L. Cheung, *J. Chem. Phys.* **135**, 054704 (2011).
 - ²⁶ H. Fan, D. E. Resasco, and A. Striolo, *Langmuir* **27**, 5264 (2011).
 - ²⁷ D. S. Frost and L. L. Dai, *Langmuir* **27**, 11339 (2011).
 - ²⁸ T. P. Bigioni, X.-M. Lin, T. T. Nguyen, E. I. Corwin, T. A. Witten, and H. M. Jaeger, *Nature Mater.* **5**, 265 (2006).
 - ²⁹ D. Wang, S. Yordanov, H. M. Paroor, A. Mukhopadhyay, C. Y. Li, H.-J. Butt, and K. Koynov, *Small* **7**, 3502 (2011).
 - ³⁰ S. Cheng, J. B. Lechman, S. J. Plimpton, and G. S. Grest, *J. Chem. Phys.* **134**, 224704 (2011).
 - ³¹ K. Kremer and G. S. Grest, *J. Chem. Phys.* **92**, 5057 (1990).
 - ³² M. K. Petersen, J. B. Lechman, S. J. Plimpton, G. S. Grest, P. J. in't Veld, and P. R. Schunk, *J. Chem. Phys.* **132**, 174106 (2010).
 - ³³ As results for the shear viscosity for $N = 10$ and 100 were not known for $r_c = 3.0\sigma$, we equilibrated systems of 25000 chains of length $N = 10$ and 2500 chains of length $N = 100$ at zero pressure and then sheared at a given shear rate. Non-equilibrium trajectories were generated by integrating the SLLOD equations of motion.³⁴ The shear viscosity η was calculated for several shear rates and extrapolated to zero shear rate. We found $\eta = 12 \pm 1$ and 180 ± 10 $m/\sigma\tau$ for $N = 10$ and 100 , respectively.
 - ³⁴ M. E. Tuckerman, C. J. Mundy, S. Balasubramanian, and M. L. Klein, *J. Chem. Phys.* **106**, 5615 (1997).
 - ³⁵ H. C. Hamaker, *Physica (Amsterdam)* **4**, 1058 (1937).
 - ³⁶ R. Everaers and M. R. Ejtehadi, *Phys. Rev. E* **67**, 041710 (2003).
 - ³⁷ P. J. in't Veld, M. K. Petersen, and G. S. Grest, *Phys. Rev. E* **79**, 021401 (2009).
 - ³⁸ G. S. Grest, Q. Wang, P. J. in't Veld, and D. J. Keffer, *J. Chem. Phys.* **134**, 144902 (2011).
 - ³⁹ Calculating θ_c as a function of A_{ns} provides a convenient way to determine the phase diagram of a nanoparticle/liquid mixture. Studies along this line will be presented in a future publication.
 - ⁴⁰ S. J. Plimpton, *J. Comp. Phys.* **117**, 1 (1995).
 - ⁴¹ <http://lammps.sandia.gov/>.
 - ⁴² B. J. Alder and T. E. Wainwright, *Phys. Rev.* **127**, 359 (1962).
 - ⁴³ K. Binder, S. Sengupta, and P. Nielaba, *J. Phys.: Condens. Matter* **14**, 2323 (2002).
 - ⁴⁴ C. H. Mak, *Phys. Rev. E* **73**, 065104 (2006).
 - ⁴⁵ P. A. Kralchevsky, N. D. Denkov, V. N. Paunov, O. D. Velev, I. B. Ivanov, H. Yoshimura, and K. Nagayama, *J. Phys.: Condens. Matter* **6**, A395 (1994).
 - ⁴⁶ J. Bleibel, A. Dominguez, M. Oettel, and S. Dietrich, *Eur. Phys. J. E* **34**, 125 (2011).
 - ⁴⁷ P. J. Steinhardt, D. R. Nelson, and M. Ronchetti, *Phys. Rev. B* **28**, 784 (1983).